International Journal of Applied Earth Observations and Geoinformation 112 (2022) 102862

Contents lists available at ScienceDirect

International Journal of Applied Earth Observations and Geoinformation

journal homepage: www.elsevier.com/locate/jag

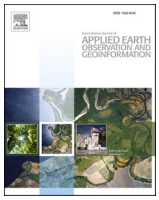

Assessing land surface phenology in Araucaria-Nothofagus forests in Chile with Landsat 8/Sentinel-2 time series

E. Kosczor [a], M. Forkel [a,*], J. Hernández [b], D. Kinalczyk [a], F. Pirotti [c], E. Kutchartt [c]

[a] Technische Universität Dresden, Institute of Photogrammetry and Remote Sensing, Helmholtzstr. 10, 01069 Dresden, Germany
[b] Universidad de Chile, Facultad de Ciencias Forestales y de la Conservación de la Naturaleza, Av. Santa Rosa, 11315 La Pintana, Santiago, Chile
[c] University of Padova, Department of Land, Environment, Agriculture and Forestry (TESAF), Via dell'Università 16, 35020 Legnaro (PD), Italy

ARTICLE INFO

Keywords:
Araucaria araucana
Land surface phenology
Plant phenology
Topography
Climate
Random Forests
Dense time series

ABSTRACT

The Araucaria-Nothofagus forests are a unique ecosystem in temperate rainforests of Chile and Argentina. They include red-listed species and have a high cultural importance for the ancestral population and thus require continuous monitoring to support conservation. Monitoring of phenology by satellite observations is a key tool to quantify the impact of climate variability on terrestrial vegetation. Here we aim to provide a first quantification and ecological understanding of the land surface phenology of protected Araucaria-Nothofagus forests in the Conguillío National Park in southern Chile. We exploit time series of enhanced vegetation index from Landsat 8 and Sentinel-2 satellite imagery from 2016 to 2020 to derive start and end-of-season (SOS and EOS) information at 10 × 10 m spatial resolution. Results show that, on average, SOS varies between 11th October and 5th November (quantiles 25% and 75% of all pixels). SOS occurs later at higher elevation, in sparsely vegetated stands, or in stands dominated by *Nothofagus antarctica*. EOS occurs on average between 24th March and 14th April. EOS shows a high variability between neighboring pixels that cannot be easily associated with forest stands or topography. Comparisons with regional-aggregated temperature and precipitation time series show that SOS is delayed with colder winter and spring temperatures and EOS shows stronger (but contrasting) correlations with summer and fall precipitation. By using a machine learning approach, we find that elevation is the main control on the spatial-temporal variability of SOS and EOS, followed by aspect, slope and total tree cover. These results suggest that meteorological conditions control the inter-annual variability of the phenology of Araucaria-Nothofagus forests but the effect is modified by small-scale topography, climate and stand characteristics.

1. Introduction

The monkey puzzle tree, *Araucaria araucana* [Mol.] K. Koch, is an endemic gymnosperm from the temperate rainforests of south-central Chile and south-western Argentina (Mundo et al., 2013). This particular species grows in association with other evergreen and deciduous southern hemisphere beech species, such as *Nothofagus pumilio* (Poepp. et Endl.) Krasser, *Nothofagus dombeyi* (Mirb.) Bl., *Nothofagus obliqua* (Mirb.) Bl., *Nothofagus antarctica* (Forst.) Oerst., among others (Kutchartt et al., 2021; Schmidt, 1977), creating an internationally unique forest composition. The importance of *A. araucana* lies in its conservation status and cultural importance. According to Drake et al. (2005), the Araucaria forest type covers around 400,000 ha between Chile and Argentina; the largest part of the area is located in Chile with 254,000 ha (Donoso et al., 2014; Molina et al., 2015). The historic coverage of *A. araucana* forest type is estimated at between 500,000 and 722,300 ha (Luebert & Pliscoff, 2018). The area has decreased because of natural disturbances and anthropogenic drivers (Burns, 1993; González et al., 2005) such as forest fires, alteration of volcanism, landslides, logging, intense livestock grazing and the overexploitation of seeds (Donoso et al., 2014; Zamorano-Elgueta et al., 2012). *A. araucana* is protected by Chilean law which prohibits its felling (Ojeda et al., 2011). At the international level, it is included in the International Union for Conservation of Nature's (IUCN) Red List of Threatened Species and is included in the Convention on International Trade in Endangered Species (CITES) (Premoli et al., 2013; Rafii & Dodd, 1998). In addition, it is considered a sacred tree by the Pewenche people (Herrmann, 2006).

Given this endemic and unique value of the Araucaria forests, monitoring this ecosystem is crucial to support its conservation status. In many ecosystems, monitoring phenological changes provides

* Corresponding author.
E-mail address: matthias.forkel@tu-dresden.de (M. Forkel).

https://doi.org/10.1016/j.jag.2022.102862
Received 25 March 2022; Received in revised form 4 June 2022; Accepted 6 June 2022
Available online 18 June 2022

information on the effect of climate change on structural and physiological changes of plants (Richardson et al., 2013). The scientific exploration of phenology has only begun to gain importance during the last few decades when its value for monitoring and evaluation of global climate change was discovered (Richardson et al., 2013). To our knowledge, there is no information of the phenology of Araucaria-Nothofagus forests and its response to climate variability based on remote sensing applications.

As in other temperate and boreal ecosystems, changes in climate variability might affect the seasonality of Araucaria-Nothofagus forests and hence productivity and growth (Buermann et al., 2018). In addition to large-scale weather conditions and climate variability, the hypothesis is that the complex topography in the Andes significantly impacts the phenology of Araucaria forests. Improving the knowledge of the spatial patterns and environmental drivers of the phenology of these protected forests is key in order to understand how future climate change and increasing anthropogenic pressure might affect these ecosystems.

The observation of phenology on a large and global scale, commonly referred to as land surface phenology (LSP), has become feasible with the emergence of satellite images in the last four decades (Helman, 2018; Liang et al., 2011). The detection of LSP itself relies on the observed variations of vegetation indices (VIs) through time, which make use of the specific reflectance characteristics of plants in various spectral bands. Consistent VI records can be used to identify the timing, length and intensity of single greening events and entire seasons. This integrative large-scale view offers many possibilities for research in a wide range of scientific fields. LSP products are important components for regional and global biosphere models and a crucial resource for monitoring and understanding climate change (Helman, 2018; Liang et al., 2011).

Generally, the estimation of phenological events relies on the detection of short time periods during which a vegetation spectral pattern changes significantly. This is only accurately possible if a time series is available that consists of a great number of data points. If large surfaces are to be analyzed and high spatial resolution is also required, only a few options remain when it comes to the choice of satellite data. Instead of limiting oneself to only one data source, combining data from different sensors is an effective method to meet these requirements, for example by the usage of harmonized Sentinel-2 (MSI) and Landsat 8 (OLI) data (e.g. Kowalski et al., 2020).

Processing data from both satellite missions increases the number of observations and possible data points, which is a novelty for the Earth observation community at this scale (Bolton et al., 2020). The three satellites, Landsat 8, Sentinel-2A and −2B have a global median average revisit interval of approximately three days, which creates more opportunities for cloud-free observations, and much denser time series (Li & Roy, 2017). When VIs are used as an indicator for phenology, inconsistencies between the wavelengths of spectral bands need to be considered – specifically the near-infrared band in this case, which differs by 29 nm between the Sentinel-2 satellites and the Landsat 8 satellite. Variations in VIs typically depend on vegetation density per pixel and the index itself. These can be minimized in preprocessing, e.g., through applying spectral harmonization algorithms (Scheffler et al., 2020).

The aim of this study is to increase the understanding of the spatial patterns and underlying environmental drivers on the phenology of protected Araucaria-Nothofagus forests. Specifically, the objectives are (1) to map the spatial and temporal variations of start of season and end of season from dense satellite time series of Landsat 8 and Sentinel-2 between 2016 and 2020 and (2) to quantify the effects of topography, temperature, and precipitation on the spatial and temporal variability of the phenometrics.

2. Materials and methods

2.1. Study area and forest inventory data

The Conguillío National Park is located in the Araucanía region of Chile in the Andes Mountain Range (Fig. 1). The park reaches altitudes of between 700 m and 3,125 m a.s.l. (peak of the Llaima volcano) (Ojeda et al., 2011). Most of the forest occurs in the valley between the Llaima volcano and Sierra Nevada volcano around Lake Conguillío (1,120 m a.s.l.). The treeline is slightly above 1,500 m a.s.l. (Veblen, 1982). The forests are a mix of *A. araucana* and at least one *Nothofagus spp*., most commonly *N. pumilio*, *N. dombeyi*, *N. antarctica* and *N. alpina*. Other species are *Chusquea* spp. and other undergrowth plants (Ojeda et al., 2011; Veblen, 1982). The diversity of Araucaria forest compositions in Conguillío National Park is substantial compared to other sites, as the high abundance of *N. dombeyi* is almost unique.

We used forest inventory data about species distribution and tree height of each stand, which were surveyed by CONAF in 2013 as part of the Native Forest Cadastre (Fig. 1). Additionally, we used the satellite-derived map of fractional tree cover from Hansen et al. (2013).

2.2. Sentinel-2 and Landsat 8 satellite data and preprocessing

Sentinel-2 (ESA, 2015) and Landsat 8 (USGS, 2019) top-of-atmosphere (TOA) radiance (Level-1) multi-spectral imagery with less than 70% cloud cover were downloaded over a time-range between 1st January 2016 and 31st December 2020. Preprocessing steps (radiometric, topographic and atmospheric correction and the adjustment of the Bidirectional Reflectance Distribution Function) were performed using the Framework for Operational Radiometric Correction for Environmental Monitoring (FORCE) (Frantz, 2019) to obtain bottom-of-atmosphere reflectance. Cloud and cloud shadow masks were also produced from the Quality Assurance Information layer provided by FORCE using the Cloud Detection Index. Sentinel-2 data was co-registered using monthly Landsat near-infrared images. Since both Sentinel-2 and Landsat 8 imagery are supposed to be analyzed together, all bands were resampled to the 10 m resolution bands of Sentinel-2, including the narrow near infrared band of Sentinel-2 (Band 8A) which is later also used in the analysis as its wavelength characteristics fit the central wavelength of the Landsat 8 near infrared band (Band 5) well. Bands 2 and 4 were used as blue and red bands from both satellite products respectively. In total, we used 378 satellite scenes, resulting in an average interval of approximately five days.

2.3. Derivation of phenological metrics

Several phenometrics and methods are available to quantify land surface phenology (de Beurs & Henebry, 2010; Forkel et al., 2015). Here, we extracted SOS and EOS with a multi-step process (Filippa et al., 2016).

First, we used the Enhanced Vegetation Index (EVI) as the most appropriate index from existing literature (Kowalski et al., 2020; Liang et al., 2011):

$$EVI = G^{*}\frac{(NIR - R)}{(NIR + C1^{*}R - C2^{*}B + L)}$$

with B, R and NIR respectively blue, red and near-infrared bands, G = 2.5 being the gain factor, L = 1 the canopy background adjustment factor, and C1 = 6 and C2 = 7.5 being the two aerosol resistance weights (Huete et al., 2002; Liu & Huete, 1995).

Second, EVI time series are smoothed with a rolling median window (width of 5 observations) to Freduce short-term variability; values below

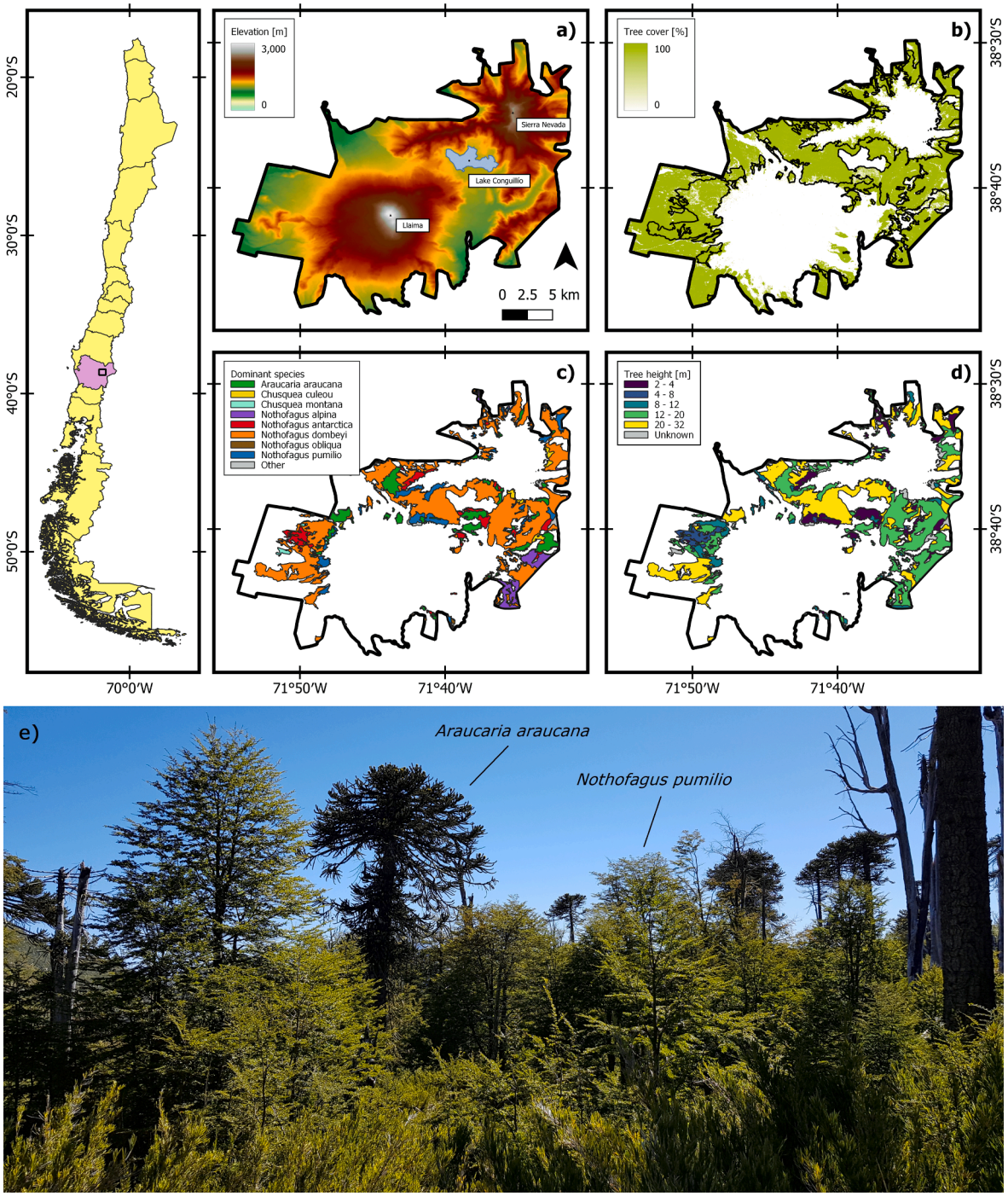

Fig. 1. Location of Conguillío National Park within Chile (pink: Araucanía Region) and illustration of (a) elevation profile (in m), (b) tree cover percentage (in %), (c) dominant species distribution, (d) tree height distribution (in m) within the park and (e) exemplary photograph of an Araucaria-Nothofagus forest in the national park. The data region in subfigures c) and d) are constrained to the stands in which *A. araucana* is present. In subfigure b) this area is outlined. (For interpretation of the references to colour in this figure legend, the reader is referred to the web version of this article.)

and above 1st and 99th percentiles were removed as considered outliers – results are shown in the gray line in Fig. 2.

Third, we interpolate time series by fitting the double logistic function by Beck et al. (2006):

$$EVI(t) = EVI_w + (EVI_m - EVI_w)*\left(\frac{1}{1+exp(-m_S*(t-S))} + \frac{1}{1+exp(m_A*(t-A))} - 1\right).$$

where t is day-of-year (DOY), EVI_w is the winter EVI, EVI_m is the maximum EVI value of the year, S and A are the spring and fall inflection points (in DOY) when the curve rises and drops, and m_S and m_A are respectively the rates of increase and decrease in spring and fall. The estimation of the six parameters was done using the implementation in the *greenbrown* package (Forkel et al., 2015).

Lastly, DOYs corresponding to SOS and EOS for each year and each pixel are extracted from the fitted curve when it crosses the 50% threshold of its annual maximum value in upward and downward direction (White et al., 1997). A limitation of threshold methods is that they might fail to accurately detect SOS and EOS when the EVI signal does not follow one clear seasonal cycle (de Beurs & Henebry, 2010); this is, however, not an issue in our study region.

2.4. Assessing environmental controls on phenology

A digital elevation model (DEM) and a meteorological dataset were used to assess environmental drivers of SOS and EOS. As DEM, we used the Shuttle Radar Topography Mission (SRTM) data with one arc-second (≈ 30 m) resolution (USGS, 2015), resampled to 10 m resolution. Slope and aspect were calculated from the elevation data using the Horn algorithm (Horn, 1981) as implemented in R raster version 3.4.10.

Gridded precipitation and minimum and maximum temperature data were taken from the meteorological reanalysis from the Chilean Center for Climate and Resilience Research (CR2MET), provided at a resolution of 0.05° (~5 km) (Boisier et al., 2018). We used monthly CR2MET data from 2016 to 2019. We aggregated the monthly precipitation and temperature time series to seasonal means in order to assess Pearson correlations with annual SOS and EOS. The seasons were defined according to the austral winter (June, July, August), spring (September, October, November), summer (December, January, February), and fall (March, April, May).

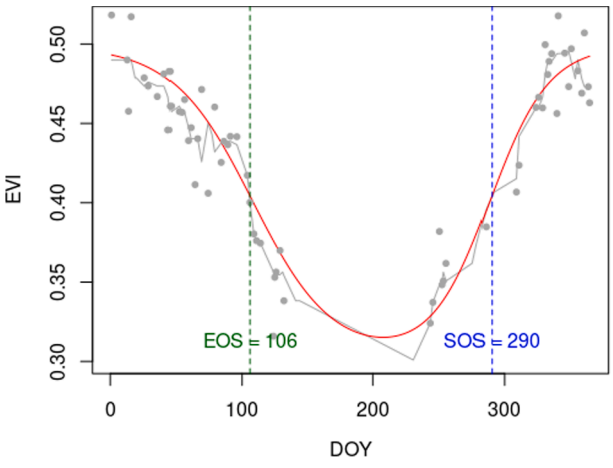

Fig. 2. Illustration of phenometrics extraction in a test pixel (38.627301°S, 71.624256°W) for 2018. Gray dots: original EVI values, gray curve: smoothed and interpolated time series, red curve: fit of double logistic model by Beck et al. (2006), blue and green: detected day of year of SOS and EOS values using the 50% threshold value of the curve fit. (For interpretation of the references to colour in this figure legend, the reader is referred to the web version of this article.)

We then used various environmental predictors in a Random Forests (RF) regression model to derive variable importance and partial relationships between each predictor and SOS or EOS. The predictors were elevation, slope, aspect, tree cover, dominant tree species, precipitation in the four seasons, and minimum, maximum and average temperature in the four seasons. The meteorological variables were taken as anomalies with respect to the multi-year mean values in order to rule out possible correlations with elevation. All datasets were resampled to 100 m resolution using bilinear interpolation as a compromise between the high spatial resolution of the phenology metrics and the low spatial resolution of the meteorological dataset. We used RF (Breiman, 2001) from the R package *randomForest* version 4.6.14 with default settings, i.e. 500 decision trees. To train the RF model, a random representative sample of 5000 pixels per year was taken as input. From the fitted RF model, the variable importance was assessed using the mean decrease accuracy measure and the partial relationships between SOS or EOS and each predictor were derived and displayed in terms of partial dependence plots (PDPs). The model results were confirmed by running a repeated 5-fold cross-validation and comparing the performance metrics.

3. Results

3.1. Spatial patterns of start-of-season

The multi-year SOS varies between DOYs 285 (11th October, 25%-ile) and 310 (5th November, 75%-ile) (Fig. 3), with high spatial variation. For example, SOS occurs at later dates in specific areas (darker green areas in Fig. 3 b-d). The stands with a later SOS than adjacent stands in the central and western regions co-occur with sparse vegetation cover, specific species and tree height. The forest stands south of Lake Conguillío are less dense and mixed with *A. araucana* together with *N. antarctica* (Fig. 1b and c). Other forests west and north of Lake Conguillío are a mix of *A. araucana* with *N. dombeyi* and *N. pumilio*. The same characteristics are visible in the western region where a dominance of *N. antarctica* experiences later SOS than surrounding forest stands in which various other species can be found. This observation also corresponds to differences in tree heights between forest stands (Fig. 1d).

While stands with later SOS in the eastern and western regions correspond to higher elevations, pixels in lower and flatter areas experience earlier SOS. The eastern region also contains a range of hills spanning to the east where differences in altitude and its effect on SOS are especially noticeable (Fig. 3d). These results indicate that topography (mainly elevation and slope) and species distribution show distinct SOS patterns.

3.2. Spatial patterns of end-of-season

The multi-year EOS varies between DOYs 84 (24th March, 25%-ile) and 105 (14th April, 75%-ile) (Fig. 4). The eastern region exhibits a notably later onset of senescence than most other areas. In contrast to the SOS, the EOS does not vary strongly between forest stands but shows higher variability at small scales between pixels. Both early and late EOS values occur within a relatively small area in several locations. This is

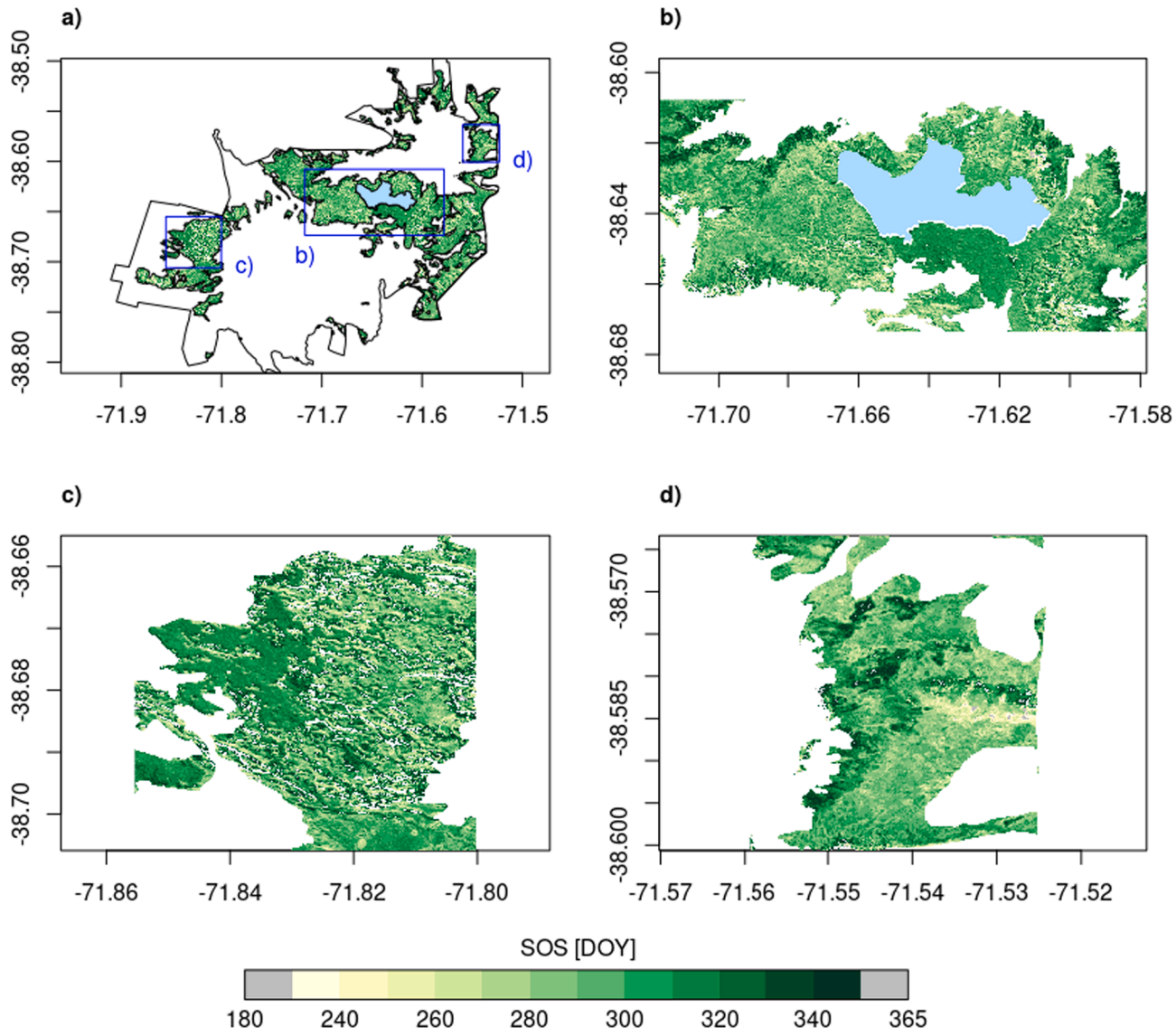

Fig. 3. Mean SOS (2016–2020) in DOY for Araucaria forests in (a) the Conguillío National Park and in the (b) central region around Lake Conguillío, (c) western region at Llaima volcano, and (d) eastern region, east of Sierra Nevada volcano.

especially apparent in the more mountainous regions east and north of Lake Conguillío and at the slopes of Llaima in the western region. In the eastern region, EOS is consistently later especially along the range of hills in the center. The small-scale variability of EOS cannot be visually related to species distribution, forest height or topography as it was for SOS.

3.3. Distribution of SOS and EOS with species composition and tree height

The spatial variability of SOS and EOS are associated with species distribution and tree height (Fig. 5). In forest stands dominated by the small shrub-like *N. antarctica*, SOS occurs almost 15 days later on average than in stands where the tall *N. dombeyi* dominate (Fig. 5a). This is confirmed by comparison against tree height: trees up to 8 m experience the average SOS around DOY 302 (28th October), the tallest stands have SOS around DOY 291 (17th October). Both above-mentioned species are not only responsible for the average tree height in their respective stands but are also associated with different forest densities. While *N. dombeyi* usually forms dense stands, *N. antarctica* mainly grows in sparsely vegetated areas. The fact that *N. antarctica* is a deciduous tree while *N. dombeyi* is an evergreen tree could also point to a relationship of SOS with leaf abscission, which is confirmed by the results for dominant *A. araucana* (evergreen) and *N. pumilio* (deciduous) configurations. The deciduous *N. alpina* shows differing SOS where it dominates, although the total forest area for this species is relatively low.

In contrast to the patterns observed for SOS, EOS does not vary much between differing forest compositions and tree heights (Fig. 5c and 5d). *N. dombeyi* and *N. antarctica*, which showed substantial differences in SOS, have EOS at almost the same time. Only *N. pumilio* has a later average EOS in stands where it dominates. The range of EOS values across all dominant species configurations only spans around six days. However, as *N. pumilio* is the predominant species at higher altitudes, elevation might be an influence factor here. EOS occurs earlier in stands with higher trees, although the differences are marginal, with only a three-day difference.

3.4. Inter-annual relations with temperature and precipitation

The temporal variability of regionally averaged SOS, EOS, and seasonal values of temperature and precipitation are shown in Fig. 6. For the comparison with SOS, seasonal temperature averages and

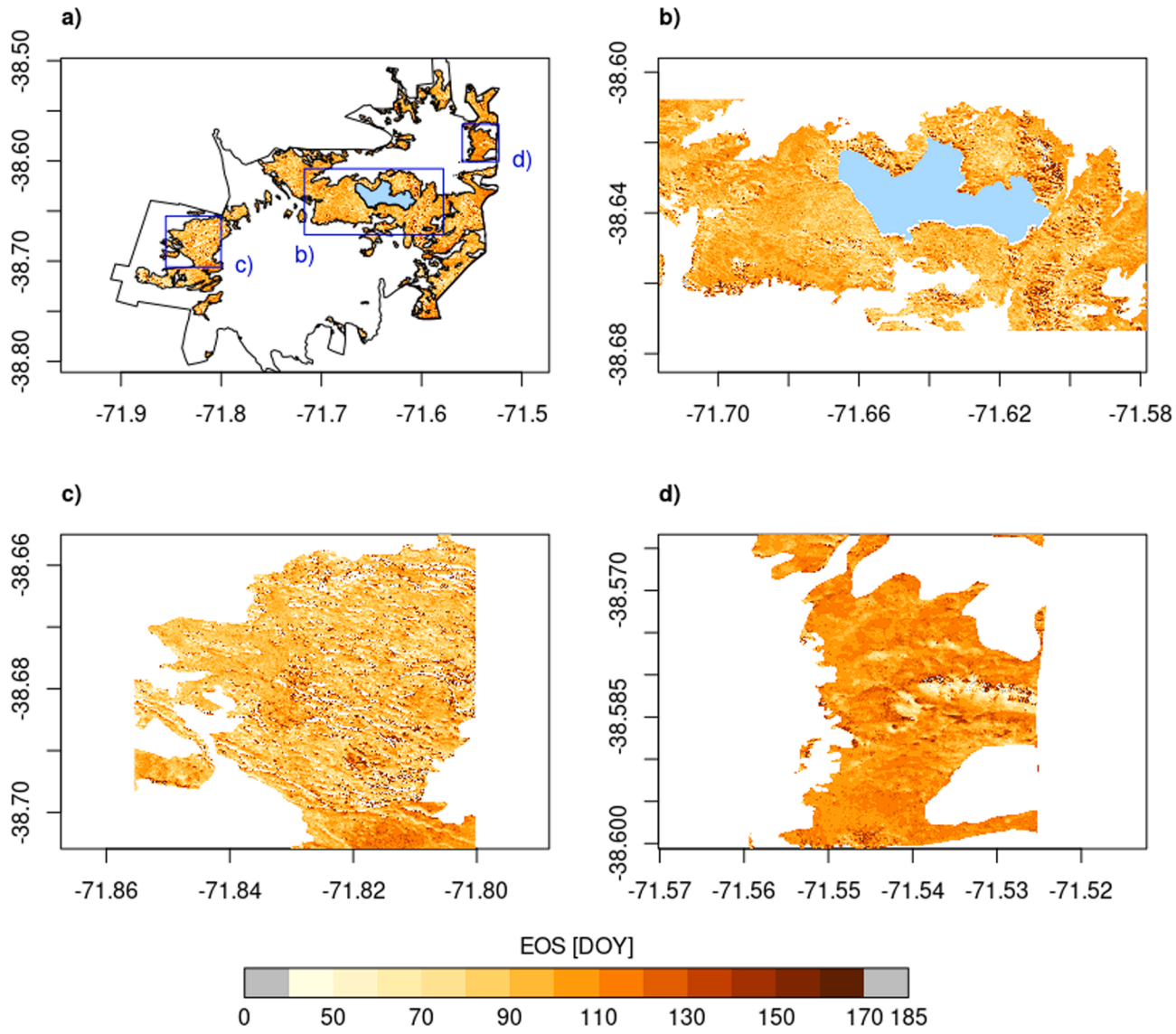

Fig. 4. Mean EOS (2016–2020) in DOY for Araucaria forests in (a) the Conguillío National Park and in the (b) central region around Lake Conguillío, (c) western region at Llaima volcano, and (d) eastern region, east of Sierra Nevada volcano.

precipitation sums are shown for winter and spring as they are expected to have a stronger influence on SOS than values from summer and fall. Likewise for the comparison with EOS, the average temperature and precipitation sums for summer and fall are shown.

The earliest SOS can be observed in 2016 (15th October) while the latest occurs in 2018 (27th October). The earliest and latest SOS in 2016 and 2018 correspond to the highest and lowest winter and spring temperature, respectively. Therefore, the inter-annual variability of SOS shows a negative correlation with winter ($r = -0.51$, $p = 0.49$) and spring ($r = -0.48$, $p = 0.52$) temperature. The latest SOS in 2018 also coincides with the highest spring precipitation which causes a positive correlation between SOS spring precipitation ($r = 0.47$, $p = 0.53$). The general course of all variables suggests that higher winter/spring average temperatures and lower spring precipitation lead to an advanced start of the growing season.

For EOS, the year 2017 stands out with a much earlier EOS (28th March) than the other years. The latest EOS occurred in 2019 (7th April). EOS shows a negative correlation with summer precipitation ($r = -0.75$, $p = 0.25$) but a positive correlation with fall precipitation ($r = 0.44$, $p = 0.56$). Interestingly, summer and fall precipitation are not correlated ($r = 0.02$, $p = 0.98$). Correlations of EOS with temperature are lower (e.g. with spring temperature: $r = 0.13$, $p = 0.87$).

SOS and EOS are positively correlated ($r = 0.71$, $p = 0.18$), suggesting that the length of the growing season is not necessarily dependent on whether the onset of greening occurs earlier or later than usual. When comparing the SOS and EOS graphs, the only growing season that stands out as longer than usual is the one starting in 2017 and ending in 2018. All in all, the results suggest that temperature and precipitation are important drivers of spring phenology in Araucaria-Nothofagus forests.

3.5. *Importance and partial relationships of phenological drivers*

The RF model was able to explain 58.1% of SOS variation (RMSE = 11 days) for the out-of-bag testing samples. Generally, the model predicts SOS well with some exceptions especially for earlier DOYs which are estimated to occur later. For EOS, RF was able to explain 49.6% of EOS variation (RMSE = 9.9 days). These results indicate that the broad spatial-temporal patterns can be predicted but both RF models underestimate the very small-scale variability.

The importance of each predictor for both SOS and EOS are shown in Fig. 7. The most relevant factor in estimating SOS and EOS is elevation.

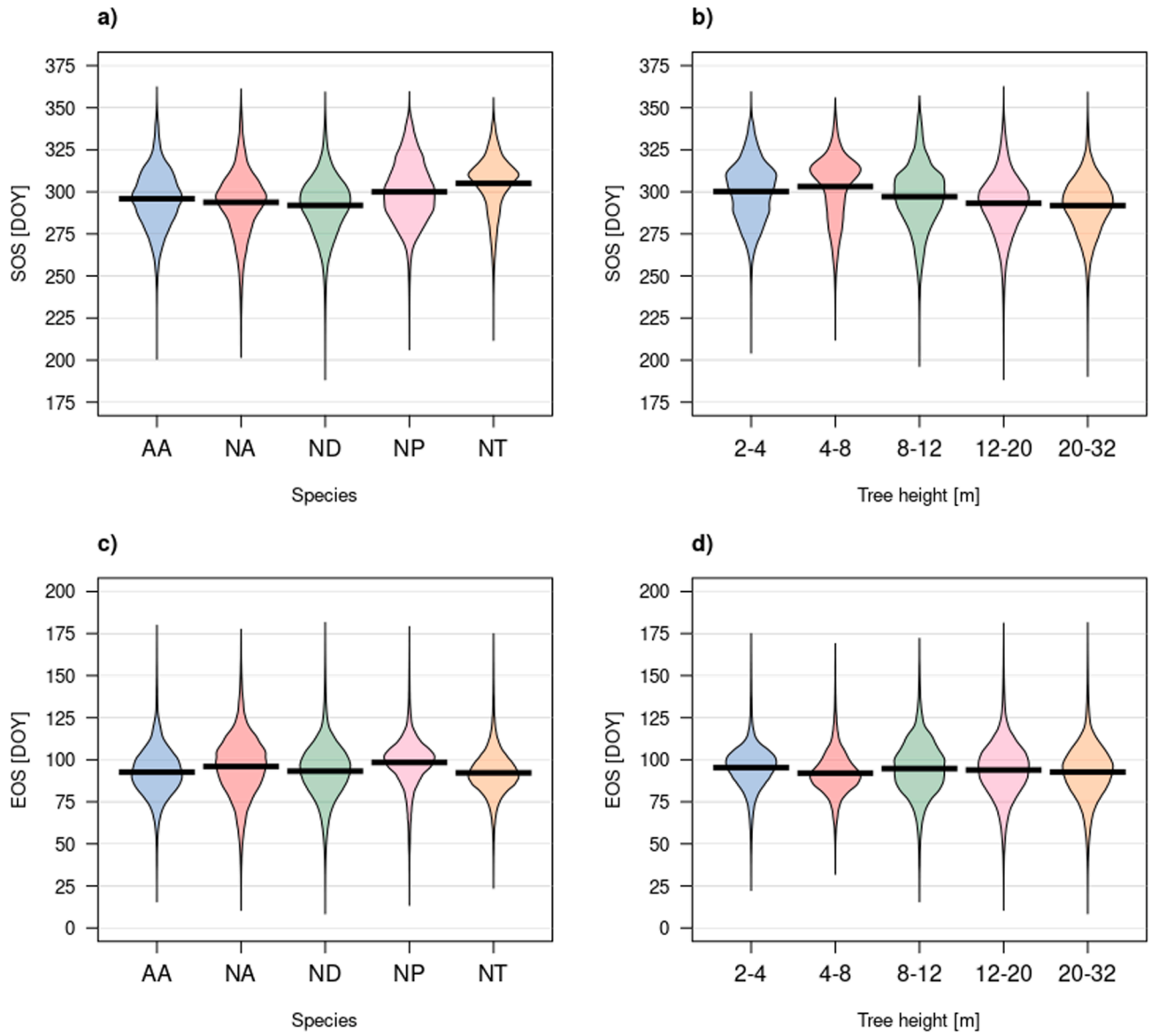

Fig. 5. Statistical distribution of start and end of season (in DOY) per forest characteristics: (a) SOS versus dominant species, (b) SOS versus tree height, (c) EOS versus dominant species and (d) EOS versus tree height. The bars represent mean values, the beans are smoothed density curves showing data distribution. The evaluated species are the five most prevalent tree species in Conguillío National Park (AA = *A. araucana*, NA = *N. alpina*, ND = *N. dombeyi*, NP = *N. pumilio*, NT = *N. antarctica*).

In both models, aspect, slope and tree cover show a high importance. For SOS, also the dominant species in a stand shows high importance. Tree height and all seasonal meteorological variables show lower importance. The results indicate that at a spatial scale of 100 × 100 m the meteorological predictors are not influential factors for SOS and EOS. The low importance for tree height suggests that the clear association with tree height as shown in Fig. 5 is rather caused by the dominant species.

The importance of elevation for the phenology of Araucaria-Nothofagus forests has been clearly demonstrated. Therefore, we now further investigate this partial relationship in terms of partial dependence plots (PDP) (Fig. 8). The PDP of SOS on elevation reveals no particular relation at lower altitudes followed by a sharp delay of SOS above 1,400 m a.s.l. Over the course of only around 250 m, the average SOS changes from DOY 294 (20th October) to DOY 306 (1st November). Similar patterns occur for the partial relation between elevation and EOS. Forest stands at higher altitudes experience a delayed EOS compared to lower areas. Here, the difference is 8 days (from 1st April to 9th April). Up until 1,300 m a.s.l., elevation has little to no effect on phenology, but becomes the main driver above these altitudes. From these results, it can be also seen that differences in elevation do not affect the overall length of the growing season.

The respective PDPs for other predictors are shown in the supporting information (Figures S1 and S2). SOS is delayed on average by 3 days at sun-shaded southern-facing slopes than at sunnier north slopes and at hillslopes $> 35°$, which again demonstrates the strong effect of topography on phenology. SOS advances with increasing tree cover, which is a relation that is likely confounded by topography because denser forests occur more in the valleys than at higher altitudes. Additionally, the PDPs reflect the previously described relations with species distribution and tree height. EOS shows relations with slope and aspect occurring earlier with increasing slope inclination. A notable difference between east- and west-facing slopes can be also observed for EOS. Overall, these results demonstrate that the large-scale variability of SOS and EOS in the region are driven by changes in meteorological conditions, but local topography is modifying those relationships.

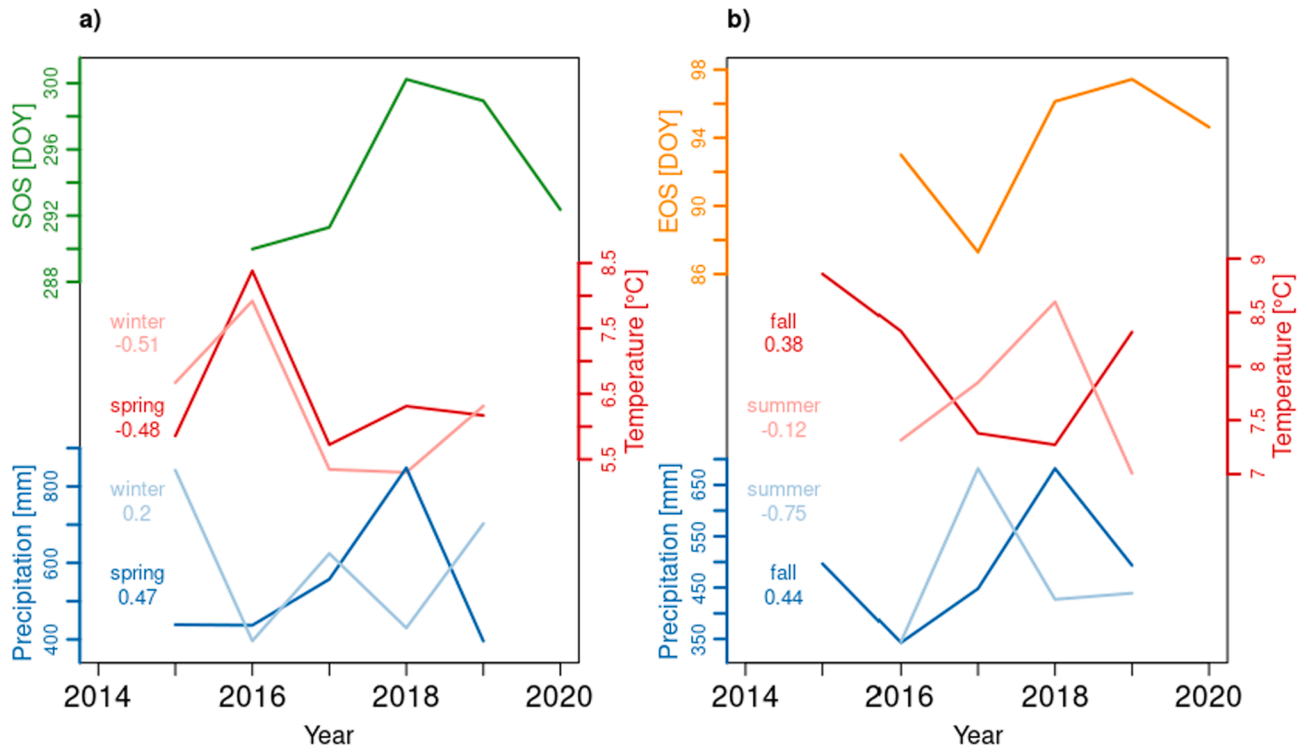

Fig. 6. Comparison of (a) mean SOS with mean average winter (JJA) and spring (SON) temperature and winter (JJA) and spring (SON) precipitation and (b) mean EOS with mean average summer (DJF) and fall (MAM) temperature and summer (DJF) and fall (MAM) precipitation in the study area (2015–2020) (n = 5). Summer data always includes December of the previous year (n = 4). Correlation of climate with phenology data is indicated to the left of the curves.

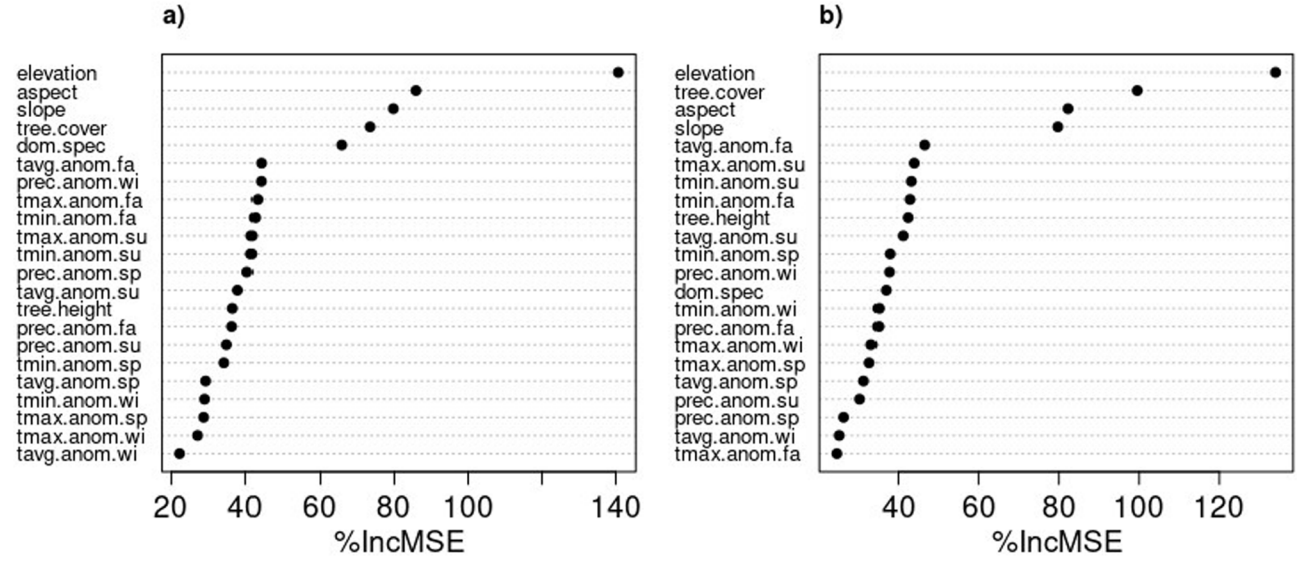

Fig. 7. Variable importance for predicting (a) SOS and (b) EOS given in percentage of MSE increase if the variable would be randomly permuted (dom.spec = dominant species, prec = precipitation, tavg = average temperature, tmax = maximum temperature, tmin = minimum temperature, anom = anomaly, sp = spring, su = summer, fa = fall, wi = winter).

4. Discussion and conclusions

Mainly the start of the season reveals clear spatial variability within the study area that can be related to species distribution and topography. While regions with a delayed SOS include sparse stands of *N. antarctica*, regions with an advanced SOS include mostly stands of *A. araucana* with *N. dombeyi* as dominant species. However, we also found that this association to species distribution is also confounded by tree height, whereby smaller trees (e.g. *N. antarctica* stands) show delayed SOS. The influence of climate on phenology is mainly visible in years with more extreme conditions and less in years with average conditions. Random Forests analysis in this study suggested that species composition is the more important predictor for phenology than tree height. Some recent studies also highlight the value of land surface phenology information to map species distribution (Aragones et al., 2019; Kollert et al., 2021), which indeed suggests that species composition is the prominent factor driving land surface phenology.

Although we found a delayed EOS with increasing elevation, EOS did

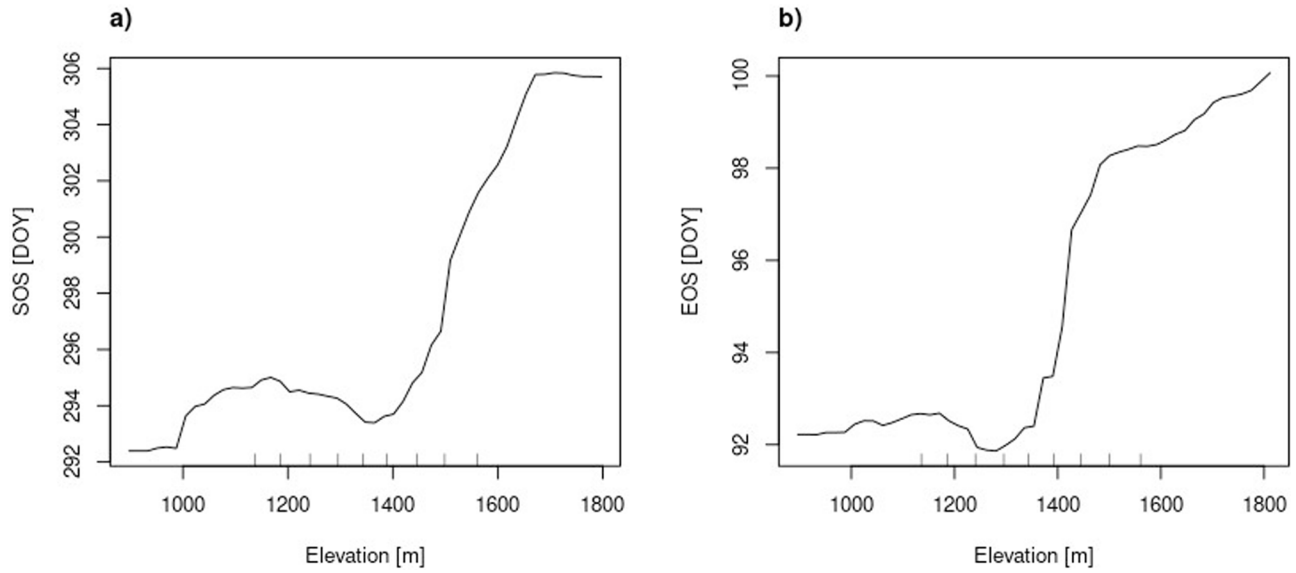

Fig. 8. Partial dependences of (a) SOS and (b) EOS (in DOY) on elevation as the variable of highest importance. Inner tick marks represent deciles of data distribution.

not show clear spatial patterns or associations with topographic patterns or species distribution (besides with *N. pumilio*). The correlation results with climatic variables indicate that the availability of rainfall in summer and fall might influence EOS but the relation is complex and seems to be affected by the high temporal variability in precipitation. Generally, fall phenology is less studied and understood than spring phenology (Chen et al., 2020). Studies from other temperate and boreal ecosystems show that fall phenology is related to various factors such as light limitation (Zhang et al., 2020), the vegetation development during the growing season (Wang et al., 2019), or to lagged drought effects and rooting patterns (Peng et al., 2019). Drought effects on trees are also strongly affected by local variations in soil texture and soil moisture, which have not been investigated within this analysis.

We found a clear year-to-year variability in SOS and EOS over the 2016–2020 period, which is correlated with seasonal temperature and precipitation conditions. The short time series of five years does not allow any statements about trends related to climate change in the long-term. A comparable analysis with coarse-resolution data over a longer period could help in identifying important trends.

For both SOS and EOS, elevation was identified by the RF models as the main driver for phenology. Our results partly confirm the generic bioclimatic law by Hopkins of 4 days delay in SOS every 120 m altitude increase or 1° latitude increase (Hopkins, 1919). An abrupt increase in the dependency of phenology on elevation was detected at around 1,300 m to 1,400 m a.s.l., with SOS and EOS getting steadily delayed with altitude above this point and being only marginally affected below. Such clear phenology differences with elevation were already described for individual species such as *N. pumilio* but not yet at landscape-scale (Mondino et al., 2019; Premoli et al., 2007; Rusch, 1993).

The results from PDPs suggest more complex interactions, as well as an effect of mixed-pixels as noted by Richardson et al. (2019). The similarity of the partial relations of SOS and EOS indicate that the length of the growing season remains unaffected throughout different elevations. Fall phenology is controlled by light availability in other temperate and mountain ecosystems (Migliavacca et al., 2008; Zhang et al., 2020). We hypothesize that the delayed EOS could be a result of more sun exposure of upper elevations in fall while valleys receive less radiation because of fog, low clouds or mountain shadows. We also assume that elevation is only an indirect driver of phenology, integrating various elevation-related effects such as local changes in insolation, temperature, snow cover, soil texture and soil depths. The longer presence of snow in higher altitudes could delay the seasonal green-up. In addition, soil quality has shown to be usually poorer at sites with *N. antarctica* (González & Veblen, 2006) and hence might control the phenology. Other processes in the study area could affect the phenology like the occurrence of fires, volcanic eruptions and droughts, which lead to different regeneration stages between stands and explicitly shape the forest structure (Dickson et al., 2021; Veblen, 1982). Droughts and fires are in turn often related to extreme climatic conditions and can be a consequence of climate change, presenting future challenges for Araucaria-Nothofagus forests (Arco Molina et al., 2016; Dickson et al., 2021). Although it is not certain that changes in growth patterns have an impact on phenology, studies in other areas could already prove the impact of climate variations, leading to prolonged growing seasons and an earlier onset of greening (Helman, 2018; IPCC, 2007; Richardson et al., 2013; Wang et al., 2019). The latter could be confirmed in this analysis as the year 2016 with higher than normal temperatures also featured an advanced SOS. The lower importance of seasonal climate variations in the RF models is most likely a result of the low resolution of the meteorological dataset and can therefore contain errors, since the diverse terrain of the study area likely features significant differences in precipitation and temperature. This also needs to be considered when evaluating the inter-annual correlations with climatic variables.

Finally, the influence of human activity is an important factor that is highly complex and therefore hard to determine accurately. Human pressure can affect the above-mentioned factors like fire frequency or introduce new challenges for the ecosystem through timber harvesting, plantation creation and overgrazing (Molina et al., 2015; Premoli et al., 2013). In this study, we studied protected Araucaria-Nothofagus forests in order to reveal the natural characteristics of this forest type. It would be desirable to have comparable phenology results available for areas subject to disturbance in order to assess possible differences. This poses a great opportunity for a continuation of this study.

The study has implications for the conservation of this endemic forest type with the endangered species of *A. araucana*. Novel forest management strategies should focus on the Araucaria-Nothofagus network as a whole and consider the observed altitudinal differences. The establishment of new conservation areas and cooperation with local companies is desirable to limit the exploitation of vulnerable stands on privately owned land. However, more data and ecological understanding is needed to accurately portray the different properties of *A. araucana* forests subject to various degrees of human alteration. This

study contributes to the research and conservation of Araucaria-Nothofagus forests in South America under ongoing climate change and human pressure.

CRediT authorship contribution statement

E. Kosczor: Conceptualization, Methodology, Software, Formal analysis, Data curation, Writing – original draft. **M. Forkel:** Conceptualization, Methodology, Software, Data curation, Writing – review & editing, Supervision, Funding acquisition. **J. Hernández:** Conceptualization, Resources, Supervision. **D. Kinalczyk:** Methodology, Software. **F. Pirotti:** Writing – review & editing. **E. Kutchartt:** Conceptualization, Resources.

Declaration of Competing Interest

The authors declare that they have no known competing financial interests or personal relationships that could have appeared to influence the work reported in this paper.

Acknowledgement

This study was funded by the Fondo de Investigación del Bosque Nativo, project 016/2019 and Ministerio de Agricultura, Gobierno de Chile y Corporación Nacional Forestal. E. Kosczor and M. Forkel acknowledge funding by the Deutsche Forschungsgemeinschaft (DFG, German Research Foundation) (FO 979/4-1). We thank the USGS and the Copernicus program and ESA for providing Landsat and Sentinel-2 imagery, respectively. We thank David Frantz for recommendations on the use of the FORCE software. We thank Christopher Marrs for proofreading.

Availability of data and material

The preprocessed Landsat and Sentinel-2 data as well as the derived phenology information is publicly available on the zenodo repository under the following DOI: 10.5281/zenodo.6447963.

Appendix A. Supplementary material

Supplementary data to this article can be found online at https://doi.org/10.1016/j.jag.2022.102862.

References

Aragones, D., Rodriguez-Galiano, V.F., Caparros-Santiago, J.A., Navarro-Cerrillo, R.M., 2019. Could land surface phenology be used to discriminate Mediterranean pine species? Int. J. Appl. Earth Obs. Geoinf. 78, 281–294. https://doi.org/10.1016/j.jag.2018.11.003.

Arco Molina, J.G., Hadad, M.A., Patón Domínguez, D., Roig, F.A., 2016. Tree age and bark thickness as traits linked to frost ring probability on *Araucaria araucana* trees in northern Patagonia. Dendrochronologia 37, 116–125. https://doi.org/10.1016/j.dendro.2016.01.003.

Beck, P.S.A., Atzberger, C., Høgda, K.A., Johansen, B., Skidmore, A.K., 2006. Improved monitoring of vegetation dynamics at very high latitudes: A new method using MODIS NDVI. Rem. Sens. Environ. 100, 321–334. https://doi.org/10.1016/j.rse.2005.10.021.

Boisier, J.P., Alvarez-Garretón, C., Cepeda, J., Osses, A., Vásquez, N., Rondanelli, R., 2018. CR2MET: A high-resolution precipitation and temperature dataset for hydroclimatic research in Chile. *Geophysical Research Abstracts*, **20**, EGU2018-19739.

Bolton, D.K., Gray, J.M., Melaas, E.K., Moon, M., Eklundh, L., Friedl, M.A., 2020. Continental-scale land surface phenology from harmonized Landsat 8 and Sentinel-2 imagery. Rem. Sens. Environ. 240, 111685. https://doi.org/10.1016/j.rse.2020.111685.

Breiman, L., 2001. Random Forests. Machine Learn. 45, 5–21. https://doi.org/10.1023/A:1010933404324.

Buermann, W., Forkel, M., O'Sullivan, M., Sitch, S., Friedlingstein, P., Haverd, V., Jain, A.K., Kato, E., Kautz, M., Lienert, S., Lombardozzi, D., Nabel, J.E.M.S., Tian, H., Wiltshire, A.J., Zhu, D., Smith, W.K., Richardson, A.D., 2018. Widespread seasonal compensation effects of spring warming on northern plant productivity. Nature 562, 110–114. https://doi.org/10.1038/s41586-018-0555-7.

Burns, B.R., 1993. Fire-Induced Dynamics of *Araucaria araucana-Nothofagus antarctica* Forest in the Southern Andes. J. Biogeogr. 20, 669. https://doi.org/10.2307/2845522.

Chen, L., Hänninen, H., Rossi, S., Smith, N.G., Pau, S., Liu, Z., Feng, G., Gao, J., Liu, J., 2020. Leaf senescence exhibits stronger climatic responses during warm than during cold autumns. Nat. Clim. Change 10, 777–780. https://doi.org/10.1038/s41558-020-0820-2.

de Beurs, K.M., Henebry, G.M., 2010. Spatio-Temporal Statistical Methods for Modelling Land Surface Phenology. In: Hudson, I.L., Keatley, M.R. (Eds.), Phenological Research. Springer, Netherlands; Dordrecht, pp. 177–208. https://doi.org/10.1007/978-90-481-3335-2_9.

Dickson, B., Fletcher, M., Hall, T.L., Moreno, P.I., 2021. Centennial and millennial-scale dynamics in *Araucaria – Nothofagus* forests in the southern Andes. J. Biogeogr. 48, 537–547. https://doi.org/10.1111/jbi.14017.

Donoso, S.R., Peña-Rojas, K., Espinoza, C., Galdames, E., Pacheco, C., 2014. Producción, permanencia y germinación de semillas de *Araucaria araucana* (Mol.) K. Koch en bosques naturales, aprovechados por comunidades indígenas del sur de Chile. Interciencia 39, 338–343.

Drake, F., Herrera, M.A., Acuña, E., 2005. Propuesta de manejo sustentable de *Araucaria araucana* (Mol. C. Koch). Bosque 26, 23–32. https://doi.org/10.4067/S0717-92002005000100003.

ESA (2015) *Sentinel-2 User Handbook* (Revision 2) ESA Standard Document; Paris, France. https://sentinel.esa.int/documents/247904/685211/Sentinel-2_User_Handbook [Accessed 17 February 2022].

Filippa, G., Cremonese, E., Migliavacca, M., Galvagno, M., Forkel, M., Wingate, L., Tomelleri, E., Morra di Cella, U., Richardson, A.D., 2016. Phenopix: A R package for image-based vegetation phenology. Agric. For. Meteorol. 220, 141–150. https://doi.org/10.1016/j.agrformet.2016.01.006.

Forkel, M., Migliavacca, M., Thonicke, K., Reichstein, M., Schaphoff, S., Weber, U., Carvalhais, N., 2015. Codominant water control on global interannual variability and trends in land surface phenology and greenness. Glob. Change Biol. 21, 3414–3435. https://doi.org/10.1111/gcb.12950.

Frantz, D., 2019. FORCE—Landsat + Sentinel-2 Analysis Ready Data and Beyond. Rem. Sens. 11, 1124. https://doi.org/10.3390/rs11091124.

González, M.E., Veblen, T.T., Sibold, J.S., 2005. Fire history of Araucaria-Nothofagus forests in Villarrica National Park, Chile. J. Biogeogr. 32, 1187–1202. https://doi.org/10.1111/j.1365-2699.2005.01262.x.

González, M.E., Veblen, T.T., 2006. Climatic influences on fire in *Araucaria araucana–Nothofagus* forests in the Andean cordillera of south-central Chile. Écoscience 13, 342–350. https://doi.org/10.2980/i1195-6860-13-3-342.1.

Hansen, M.C., Potapov, P.V., Moore, R., Hancher, M., Turubanova, S.A., Tyukavina, A., Thau, D., Stehman, S.V., Goetz, S.J., Loveland, T.R., Kommareddy, A., Egorov, A., Chini, L., Justice, C.O., Townshend, J.R.G., 2013. High-Resolution Global Maps of 21st-Century Forest Cover Change. Science 342 (6160), 850–853.

Helman, D., 2018. Land surface phenology: What do we really 'see' from space? Sci. Total Environ. 618, 665–673. https://doi.org/10.1016/j.scitotenv.2017.07.237.

Herrmann, T.M., 2006. Indigenous Knowledge and Management of *Araucaria Araucana* Forest in the Chilean Andes: Implications for Native Forest Conservation. Biodivers. Conserv. 15, 647–662. https://doi.org/10.1007/s10531-005-2092-6.

Hopkins, A.D., 1919. The Bioclimatic Law as Applied to Entomological Research and Farm Practise. Sci. Monthly 8, 496–513.

Horn, B.K.P., 1981. Hill shading and the reflectance map. Proc. IEEE 69, 14–47. https://doi.org/10.1109/PROC.1981.11918.

Huete, A., Didan, K., Miura, T., Rodriguez, E.P., Gao, X., Ferreira, L.G., 2002. Overview of the radiometric and biophysical performance of the MODIS vegetation indices. Rem. Sens. Environ. 83, 195–213. https://doi.org/10.1016/S0034-4257(02)00096-2.

IPCC, 2007. In: Climate Change 2007: Impacts, Adaptation and Vulnerability. Contribution of Working Group II to the Fourth Assessment Report of the Intergovernmental Panel on Climate Change. Cambridge University Press, Cambridge, UK.

Kollert, A., Bremer, M., Löw, M., Rutzinger, M., 2021. Exploring the potential of land surface phenology and seasonal cloud free composites of one year of Sentinel-2 imagery for tree species mapping in a mountainous region. Int. J. Appl. Earth Obs. Geoinf. 94, 102208. https://doi.org/10.1016/j.jag.2020.102208.

Kowalski, K., Senf, C., Hostert, P., Pflugmacher, D., 2020. Characterizing spring phenology of temperate broadleaf forests using Landsat and Sentinel-2 time series. Int. J. Appl. Earth Obs. Geoinf. 92, 102172. https://doi.org/10.1016/j.jag.2020.102172.

Kutchartt, E., Gayoso, J., Pirotti, F., Bucarey, A., Guerra, J., Hernández, J., Corvalán, P., Drápela, K., Olson, M., Zwanzig, M., 2021. Aboveground tree biomass of *Araucaria araucana* in southern Chile: measurements and multi-objective optimization of biomass models. IForest – Biogeosci. Forest. 14, 61–70. https://doi.org/10.3832/ifor3492-013.

Li, J., Roy, D., 2017. A Global Analysis of Sentinel-2A, Sentinel-2B and Landsat-8 Data Revisit Intervals and Implications for Terrestrial Monitoring. Rem. Sens. 9, 902. https://doi.org/10.3390/rs9090902.

Liang, L., Schwartz, M.D., Fei, S., 2011. Validating satellite phenology through intensive ground observation and landscape scaling in a mixed seasonal forest. Remote Sens. Environ. 115, 143–157. https://doi.org/10.1016/j.rse.2010.08.013.

Liu, H.Q., Huete, A., 1995. A feedback based modification of the NDVI to minimize canopy background and atmospheric noise. IEEE Trans. Geosci. Remote Sens. 33, 457–465. https://doi.org/10.1109/36.377946.

Luebert, F., Pliscoff, P., 2018. *Sinopsis Bioclimática y Vegetacional de Chile*. Editorial Universitaria, Santiago, Chile.

Migliavacca, M., Cremonese, E., Colombo, R., Busetto, L., Galvagno, M., Ganis, L., Meroni, M., Pari, E., Rossini, M., Siniscalco, C., Morra di Cella, U., 2008. European larch phenology in the Alps: can we grasp the role of ecological factors by combining field observations and inverse modelling? Int. J. Biometeorol. 52, 587–605. https://doi.org/10.1007/s00484-008-0152-9.

Molina, J.R., Martín, A., Drake, F., Martín, L.M., Herrera, M.A., 2015. Fragmentation of *Araucaria araucana* forests in Chile: quantification and correlation with structural variables. IForest – Biogeosci. Forest. 9, 244–252. https://doi.org/10.3832/ifor1399-008.

Mondino, V.A., Pastorino, M.J., Gallo, L.A., 2019. Variación altitudinal de caracteres fenológicos y crecimiento inicial en condiciones controladas entre poblaciones de *Nothofagus pumilio* provenientes del Centro-Oeste de Chubut, Argentina. Bosque 40, 87–94. https://doi.org/10.4067/S0717-92002019000100087.

Mundo, I.A., Kitzberger, T., Roig Juñent, F.A., Villalba, R., Barrera, M.D., 2013. Fire history in the *Araucaria araucana* forests of Argentina: human and climate influences. Int. J. Wildland Fire 22, 194. https://doi.org/10.1071/WF11164.

Ojeda, N., Sandoval, V., Soto, H., Casanova, J.L., Herrera, M.A., Morales, L., Espinosa, A., San Martín, J., 2011. Discriminación de bosques de *Araucaria araucana* en el Parque Nacional Conguillío, centro-sur de Chile, mediante datos Landsat TM. Bosque 32, 113–125. https://doi.org/10.4067/S0717-92002011000200002.

Peng, J., Wu, C., Zhang, X., Wang, X., Gonsamo, A., 2019. Satellite detection of cumulative and lagged effects of drought on autumn leaf senescence over the Northern Hemisphere. Glob. Change Biol. 25, 2174–2188. https://doi.org/10.1111/gcb.14627.

Premoli, A.C., Quiroga, P. & Gardner, M.F. (2013) *Araucaria araucana*. *The IUCN Red List of Threatened Species 2013*, e.T31355A2. doi: 10.2305/IUCN.UK.2013-1.RLTS.T31355A2805113.en.

Premoli, A.C., Raffaele, E., Mathiasen, P., 2007. Morphological and phenological differences in *Nothofagus pumilio* from contrasting elevations: Evidence from a common garden. Austral Ecol. 32, 515–523. https://doi.org/10.1111/j.1442-9993.2007.01720.x.

Rafii, Z.A., Dodd, R.S., 1998. Genetic diversity among Coastal and Andean natural populations of *Araucaria araucana* (Molina) K. Koch. Biochem. System. Ecol. 26, 441–451. https://doi.org/10.1016/S0305-1978(97)00125-7.

Richardson, A.D., Keenan, T.F., Migliavacca, M., Ryu, Y., Sonnentag, O., Toomey, M., 2013. Climate change, phenology, and phenological control of vegetation feedbacks to the climate system. Agric. For. Meteorol. 169, 156–173. https://doi.org/10.1016/j.agrformet.2012.09.012.

Richardson, A.D., Hufkens, K., Li, X., Ault, T.R., 2019. Testing Hopkins' Bioclimatic Law with PhenoCam data. Appl. Plant Sci. 7, e1228. https://doi.org/10.1002/aps3.1228.

Rusch, V.E., 1993. Altitudinal variation in the phenology of *Nothofagus pumilio* in Argentina. Rev. Chil. Hist. Nat. 66, 131–141.

Scheffler, D., Frantz, D., Segl, K., 2020. Spectral harmonization and red edge prediction of Landsat-8 to Sentinel-2 using land cover optimized multivariate regressors. Remote Sens. Environ. 241, 111723. https://doi.org/10.1016/j.rse.2020.111723.

Schmidt, H., 1977. Dinámica de un bosque virgen de Araucaria – Lenga (Chile). Bosque 2, 3–11. https://doi.org/10.4206/bosque.1977.v2n1-02.

USGS, 2015. USGS EROS Archive - Digital Elevation - Shuttle Radar Topography Mission (SRTM) 1 Arc-Second Global USGS EROS. Doi: 10.5066/F7PR7TFT.

USGS, 2019. *Landsat 8 (L8) Data Users Handbook* USGS EROS; Sioux Falls, United States. https://prd-wret.s3-us-west-2.amazonaws.com/assets/palladium/production/atoms/files/LSDS-1574_L8_Data_Users_Handbook-v5.0.pdf [Accessed 17 February 2022].

Veblen, T.T., 1982. Regeneration Patterns in *Araucaria araucana* Forests in Chile. J. Biogeogr. 9, 11. https://doi.org/10.2307/2844727.

Wang, X., Xiao, J., Li, X., Cheng, G., Ma, M., Zhu, G., Altaf Arain, M., Andrew Black, T., Jassal, R.S., 2019. No trends in spring and autumn phenology during the global warming hiatus. Nat. Commun. 10, 1–10. https://doi.org/10.1038/s41467-019-10235-8.

White, M.A., Thornton, P.E., Running, S.W., 1997. A continental phenology model for monitoring vegetation responses to interannual climatic variability. Global Biogeochem. Cycles 11, 217–234. https://doi.org/10.1029/97GB00330.

Zamorano-Elgueta, C., Cayuela, L., González-Espinosa, M., Lara, A., Parra-Vázquez, M.R., 2012. Impacts of cattle on the South American temperate forests: Challenges for the conservation of the endangered monkey puzzle tree (*Araucaria araucana*) in Chile. Biol. Conserv. 152, 110–118. https://doi.org/10.1016/j.biocon.2012.03.037.

Zhang, Y., Commane, R., Zhou, S., Williams, A.P., Gentine, P., 2020. Light limitation regulates the response of autumn terrestrial carbon uptake to warming. Nat. Clim. Change 10, 739–743. https://doi.org/10.1038/s41558-020-0806-0.